Bone 84 (2016) 279–288

Contents lists available at ScienceDirect

Bone

journal homepage: www.elsevier.com/locate/bone

Original Full Length Article

Osteocyte-directed bone demineralization along canaliculi

Nobuhito Nango [a], Shogo Kubota [a], Tomoka Hasegawa [b], Wataru Yashiro [c], Atsushi Momose [c], Koichi Matsuo [d,*]

[a] Ratoc System Engineering Co., Ltd, Tokyo 112-0014, Japan
[b] Department of Developmental Biology of Hard Tissue, Hokkaido University Graduate School of Dental Medicine, Sapporo 060-8586, Japan
[c] Institute of Multidisciplinary Research for Advanced Materials, Tohoku University, Miyagi 980-8577, Japan
[d] Laboratory of Cell and Tissue Biology, Keio University School of Medicine, Tokyo 160-8582, Japan

ARTICLE INFO

Article history:
Received 7 August 2015
Revised 30 November 2015
Accepted 16 December 2015
Available online 17 December 2015

Keywords:
Demineralization/remineralization
Mineral metabolism
Osteocytic osteolysis
Osteocyte canaliculus
Synchrotron radiation
Talbot-defocus multiscan tomography

ABSTRACT

The mammalian skeleton stores calcium and phosphate ions in bone matrix. Osteocytes in osteocyte lacunae extend numerous dendrites into canaliculi less than a micron in diameter and which are distributed throughout bone matrix. Although osteoclasts are the primary bone-resorbing cells, osteocytes also reportedly dissolve hydroxyapatite at peri-lacunar bone matrix. However, robust three-dimensional evidence for peri-canalicular bone mineral dissolution has been lacking. Here we applied a previously reported Talbot-defocus multiscan tomography method for synchrotron X-ray microscopy and analyzed the degree of bone mineralization in mouse cortical bone around the lacuno–canalicular network, which is connected both to blood vessels and the peri- and endosteum. We detected cylindrical low mineral density regions spreading around canaliculi derived from a subset of osteocytes. Transmission electron microscopy revealed both intact and demineralized bone matrix around the canaliculus. Peri-canalicular low mineral density regions were also observed in osteopetrotic mice lacking osteoclasts, indicating that osteoclasts are dispensable for peri-canalicular demineralization. These data suggest demineralization can occur from within bone through the canalicular system, and that peri-canalicular demineralization occurs not uniformly but directed by individual osteocytes. Blockade of peri-canalicular demineralization may be a therapeutic strategy to increase bone mass and quality.

1. Introduction

Calcium and phosphate ions are essential for life, as they function universally in intracellular signal transduction [1] and, in vertebrate bone, crystallize into hydroxyapatite within collagen fibrils. Calcium and phosphate homeostasis in mammals is dynamically maintained by vitamin D, parathyroid hormone (PTH), fibroblast growth factor-23, and other humoral factors, which regulate cross-talk between bone and distant organs, including small intestine, kidney, parathyroid gland, and pancreas [2,3]. Adult skeletal bones constantly undergo resorption in response to calcium deficiency, loss of mechanical stress, or inflammation. Osteoclasts, which are derived from hematopoietic precursors, are the primary bone-resorbing cells. They dissolve biological apatite by secreting hydrochloric acid and break down collagen fibers by secreting the protease cathepsin K from their ruffled border onto bone surface. Osteoclastic bone resorption is usually followed by osteoblastic bone formation through coupling mechanisms [4,5]. Unbalanced, excess bone resorption results in bone loss diseases such as postmenopausal or glucocorticoid-induced osteoporosis [6–8].

Osteocytes in bone matrix are derived from bone-forming osteoblasts, which embed themselves in lacunae [9–11] and extend dendritic processes into osteocyte canaliculi. The average diameter of these processes is 104 ± 69 nm and that of canaliculi is 259 ± 129 nm [12]. Osteocytes form a syncytium in the lacuno–canalicular system and are interconnected through gap junctions at the tips of their dendritic processes. The extracellular space within canaliculi is accessible to blood in peripheral vessels, as demonstrated by rapid staining of canaliculi after intravenous injection of fluorescent dye [13]. Osteocytes produce the receptor activator of NF-κB (RANKL) and sclerostin, which, respectively, regulate osteoclast and osteoblast differentiation [14,15]. Osteocytes are abundant in bone and comprise 95% of all bone cells [11]. They are thought to dissolve bone mineral directly through acidification around osteocytic lacunae [16–18].

Synchrotron X-ray tomography is a promising technology to image osteocytic lacunae and canaliculi in undecalcified bone specimens [19–25]. Recently, peri-lacunar and peri-canalicular hypermineralization was observed using synchrotron radiation phase-contrast computed tomography (CT) [26]. However, the existence of peri-canalicular demineralization by osteocytic dendrites has not been supported by three-dimensional (3D) data.

* Corresponding author at: Laboratory of Cell and Tissue Biology, Keio University School of Medicine, 35 Shinanomachi, Shinjuku, Tokyo 160-8582, Japan.
E-mail addresses: nango@ratoc.co.jp (N. Nango), s-kubota@ratoc.co.jp (S. Kubota), hasegawa@den.hokudai.ac.jp (T. Hasegawa), wyashiro@tagen.tohoku.ac.jp (W. Yashiro), momose@tagen.tohoku.ac.jp (A. Momose), kmatsuo@keio.jp (K. Matsuo).

http://dx.doi.org/10.1016/j.bone.2015.12.006

To accurately assess function of canaliculi in demineralization within cortical bone, an imaging method must meet four requirements. First, canaliculi position must be visualized. Second, differences in the degree of mineralization around canaliculi over several microns must be quantified. Third, these properties should be observed three-dimensionally. Fourth, these parameters should be observable over a wide range (several tens of microns) covering multiple osteocytes connected with canaliculi. To this end, we developed a Talbot-defocus multiscan tomography system using synchrotron X-ray microscopy [27]. This method is currently the only one available that meets these four requirements. By contrast, fluorescence imaging and optical microscopy allow detection of canaliculi [10] but not the degree of mineralization; furthermore, transmission electron microscopy can determine the degree of mineralization but cannot generate 3D images, and the field of view is limited. Finally, scanning electron microscopy is not sensitive enough to detect differences in the degree of mineralization.

Combining Talbot-defocus multiscan tomography with transmission electron microscopy, we now provide direct evidence that osteocytes dissolve bone mineral through canaliculi, and that bone demineralization around canaliculi is regulated at the level of individual osteocytes.

2. Materials and methods

2.1. Mice and trimming of tibial cortical bone

Wild-type C57BL/6J mice were purchased from Clea Japan (Tokyo, Japan). Mice lacking c-Fos (*Fos*$^{-/-}$ mice) [28] were generated by mating of heterozygotes on a C57BL6J/129 mixed background. Mice lacking RANKL (*Tnfsf11*$^{-/-}$) were likewise generated by mating heterozygotes on a C57BL/6J background [29]. Seven-week-old C57BL/6J mice were infused with human PTH 1–34 (Peptide Institute, Inc., Osaka, Japan) at 40 μg/kg/day for 6 days using an implantable osmotic pump (ALZET model 1007D, Durect Corporation, Cupertino, CA, USA). Age-matched controls were left untreated. Tibial cortical bone was prepared as described [27]. Briefly, tibiae were embedded in LR white resin (Electron Microscopy Sciences, Fort Washington, PA, USA). The posterior cortex of the tibial diaphysis was cut longitudinally and ground into a 300 μm-wide columnar shape with intact endosteum and periosteum surfaces and then glued onto a sample rod.

Fibulae were prepared on the 12th day of lactation from 14-week-old C57BL/6J mice. Age-matched virgin mice served as controls. Fibulae were imaged at 1 mm above the distal tibiofibular junction. Experiments were carried out in accordance with the Institutional Guidelines on Animal Experimentation at Keio University and were approved by Keio University Institutional Animal Care and Use Committee.

2.2. Talbot-defocus multiscan X-ray tomographic microscopy

Talbot-defocus multiscan X-ray microscopy was performed as previously described using a monochromatic light beam of 9 keV at the beamline 20XU at the synchrotron radiation light facility SPring-8 (Hyogo, Japan) [27]. Briefly, for X-ray microscopy, a Fresnel Zone Plate (FZP-S86/416, NTT-AT, Tokyo, Japan) was used as an X-ray magnification lens. The distance between the sample and the charge-coupled device (CCD) camera was approximately 6 m. Microscopy magnification was 20.9× and pixel resolution was 0.208 μm. The matrix size of the CCD camera was 1344 × 1024 pixels. Using synchrotron X-ray tomographic microscopy, an identical region of each sample was scanned using Talbot and defocus phase-contrast methods. Talbot analysis was performed "on focus" with a Talbot interferometer consisting of two gratings [30,31]. After removing the interferometer, a defocus phase-contrast method was performed by shifting the lens downstream by 6 mm [27]. Spatial resolution was about 1 μm for Talbot phase-contrast [31] and was submicron for defocus phase-contrast tomography.

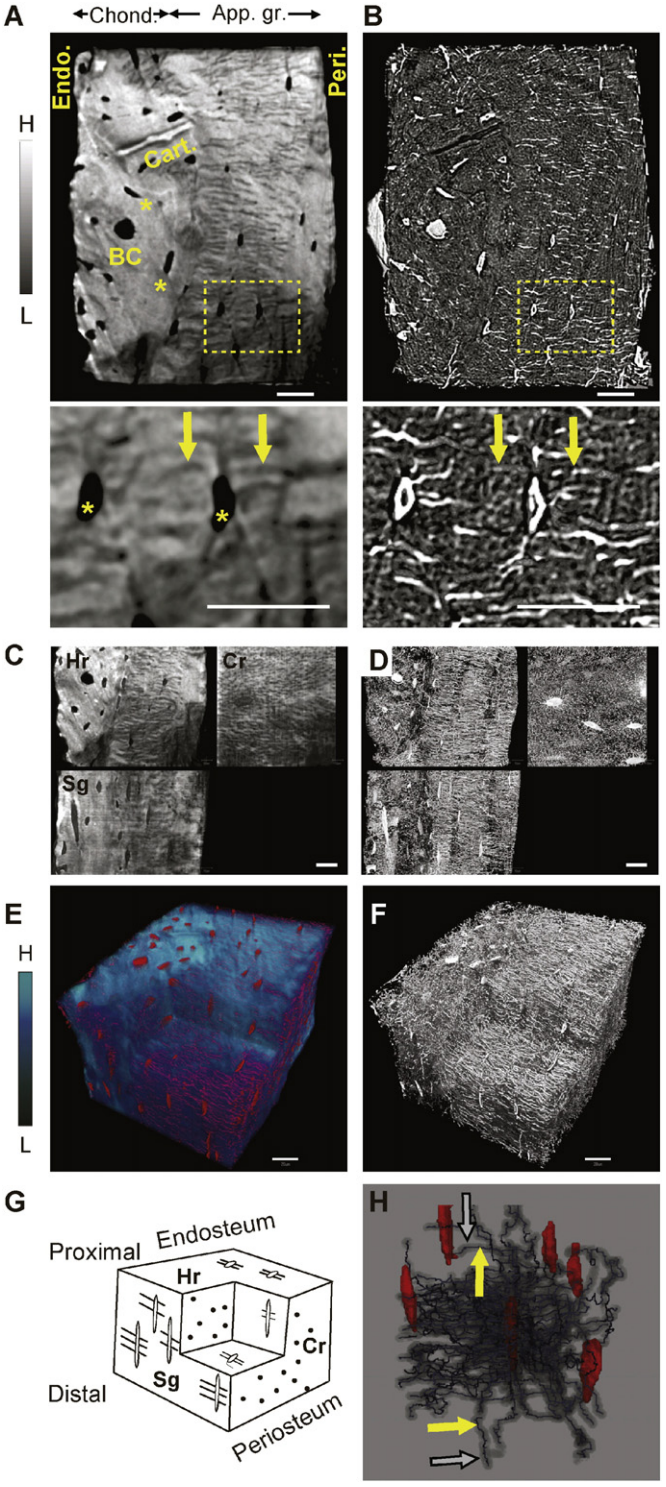

Fig. 1. Synchrotron X-ray tomographic images of tibial diaphyseal cortex in 4-week-old wild-type mice. A. Degree of mineralization depicted as grayscale (H, high mineralization; L, low mineralization) obtained by Talbot phase-contrast imaging. Endo., endosteum. Peri., periosteum. Chond., endochondral ossification. App. gr., appositional growth. Cart. Cartilage. BC, bone canal. Boxed region is enlarged in the bottom panel. Asterisks, osteocyte lacuna. Arrows, osteocyte canaliculus. B. Osteocytic lacunae and canaliculi observed by defocus phase-contrast. Boxed region is enlarged in the bottom panel. C, D. Multiplanar images (Hr, horizontal, Cr, coronal, Sg, sagittal) for Talbot (C) and defocus (D) phase-contrast. E. 3D overlay image showing degree of mineralization (Blue scale: H, high mineralization; L, low mineralization) as revealed by Talbot phase-contrast and the lacuno–canalicular system, obtained by defocus phase-contrast (red). F. The canalicular network corresponding to (E). G. Schematic representation of multiplanar images. H. Canalicular network with central canaliculi (yellow arrows) and cylindrical mineral dissolution (gray arrows) originating from one osteocyte lacuna (red, center) and five lacunae connected to it (red, in periphery). Scale bars, 20 μm.

Talbot phase-contrast method can also measure the refractive index (δ). Thus, the degree of mineralization (mg/cm^3) was determined by assuming that bone consists of hydroxyapatite and that degree of mineralization (apparent density, ρ_{app}) could be calculated as:

$$\rho_{app} = (\text{HA density}/\text{HA } \delta)(\text{observed } \delta),$$

where HA density = 3160 mg/cm^3 and HA $\delta = 8.169 \times 10^{-6}$.

2.3. Image analysis

To locate the lacuno–canalicular system, black and white (gray) scales of the defocus image were inverted. CT images reconstructed from the multiscan method were aligned in 3D space and analyzed using TRI/3D-BON software (Ratoc, Tokyo, Japan).

2.4. Transmission electron microscopy

Tibiae were dissected free of soft tissues and immersed for 18 h in 2% paraformaldehyde/2.5% glutaraldehyde in 0.1 M cacodylate buffer (pH 7.4) at 4 °C. Fixed samples were post-fixed in OsO_4, dehydrated, and embedded in epoxy resin (Epon 812, Taab, Berkshire, UK). Ultrathin sections were obtained using an ultra microtome (Sorvall MT-5000; Ivan Sorvall, Inc., Norwalk, CT, USA) and observed using a transmission electron microscope (Hitachi H-7000, Hitachi Co., Tokyo, Japan) at 80 kV.

3. Results

3.1. Synchrotron X-ray tomographic imaging of diaphyseal cortex

To assess osteocytic mineral metabolism, we analyzed bone samples for bone mineral density distribution around the lacuno–canalicular system. To this end, we prepared cortical bone samples from young (4-week-old) and mature (14-week-old) mice (Fig. 1, Supplemental Fig. S1). The posterior cortex of the tibial diaphysis was cut into rectangular prism-like blocks (~300 μm x ~ 300 μm x ~ 3 mm) with intact periosteum (the outer surface) and endosteum (the inner surface). These samples were prepared to fit into a limited view field of synchrotron X-ray tomographic microscopy in order to gain high resolution. We analyzed each sample twice, first using the Talbot effect in differential phase-contrast to reveal degree of mineralization, and then using defocus phase-contrast to visualize the lacuno–canalicular system by enhancing structural edges [27]. After reconstructing 3D images of cortical bone for both Talbot and defocus phase-contrast, we generated two images corresponding to an identical horizontal section from the two different methods (Fig. 1 A and B). In Talbot phase-contrast, bone canals (BCs), which contain blood vessels, and osteocyte lacunae (asterisks) were visualized as having the lowest grayscale values, whereas highly mineralized, persistent cartilage (Cart.) showed the highest grayscale values (Fig. 1A). In the periosteal half, osteocyte lacunae were regularly arranged, and numerous dark-gray lines (arrows) corresponding to canaliculi extended towards periosteal or endosteal surfaces from lacunae, indicating that appositional growth had occurred along the periosteum, an activity that would increase bone diameter [32] (Fig. 1A, App. gr).

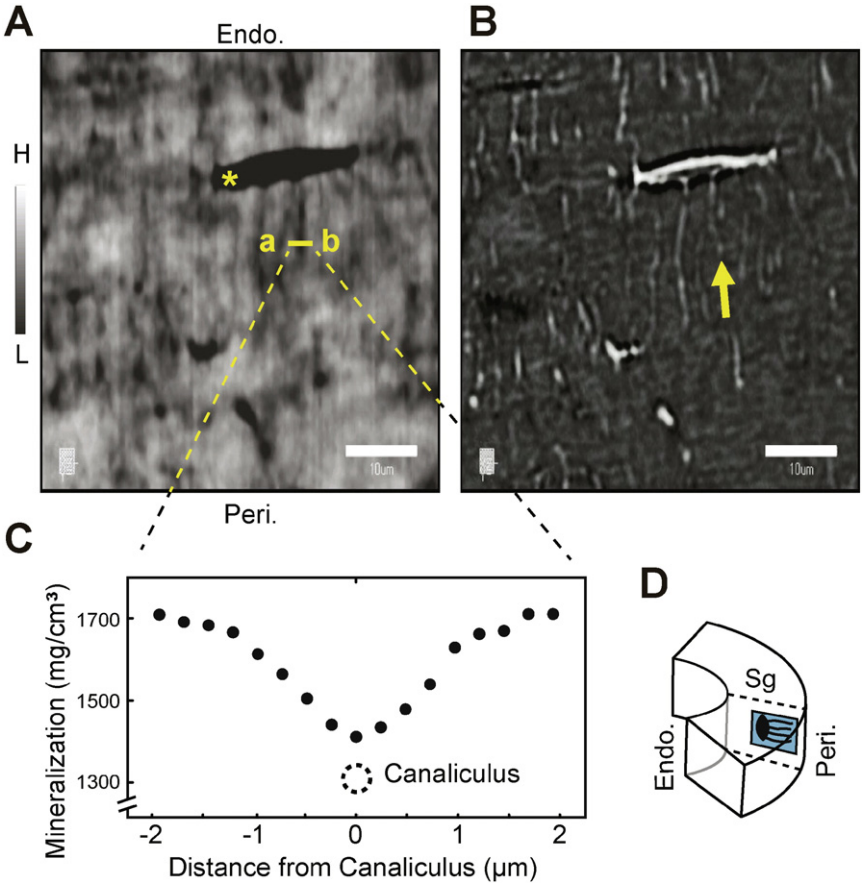

Fig. 2. Sagittal section parallel to canaliculi near the periosteal surface. A. Talbot phase-contrast image. Asterisk, osteocyte lacuna. The degree of mineralization of line a-b was quantified. H, high mineralization; L, low mineralization. Endo., endosteum. Peri., periosteum. B. Defocus phase-contrast image. Arrow, canaliculus. Scale bar, 10 μm. C. Mineralization distribution on the a-b line shown in (A), resembling a "V-shaped valley". Diameter of canaliculi (dotted circle) ranges from 0.13 to 0.39 μm [12]. D. Images in (A) and (B) were generated at the identical position in the sagittal plane (Sg).

By contrast, persistence of cartilage and irregular orientations of canaliculi suggested that the endosteal half was derived from endochondral ossification (Fig. 1A, Chond.). Defocus phase-contrast image at the same site confirmed the position of the lacuno–canalicular system (Fig. 1B).

We next examined aligned 3D images in three orthogonal planes (horizontal, sagittal and coronal; see Fig. 1G) by generating 50 μm-thick stacks of each slice for both Talbot (Fig. 1C) and defocus (Fig. 1D) phase contrast. This analysis revealed various fine structures within the posterior cortex of the tibia. Near the periosteal surface, both horizontal and sagittal planes were parallel to canaliculi, while the coronal plane was perpendicular to canaliculi, as indicated by point-like cross sections (Fig. 1C, D, and G). Talbot and defocus phase-contrast images drawn in 3D allowed us to superimpose the degree of mineralization in blue scale with the lacuno–canalicular system in red (Fig. 1E). Such analysis indicated that a zone of low mineralization includes multiple osteocyte lacunae and their canaliculi (Fig. 1E, and F). One osteocyte lacuna was connected to multiple lacunae through an osteocytic canalicular network (see five neighboring osteocytes in Fig. 1H), providing a structural basis for potential concerted activity of multiple osteocytes in mineral metabolism.

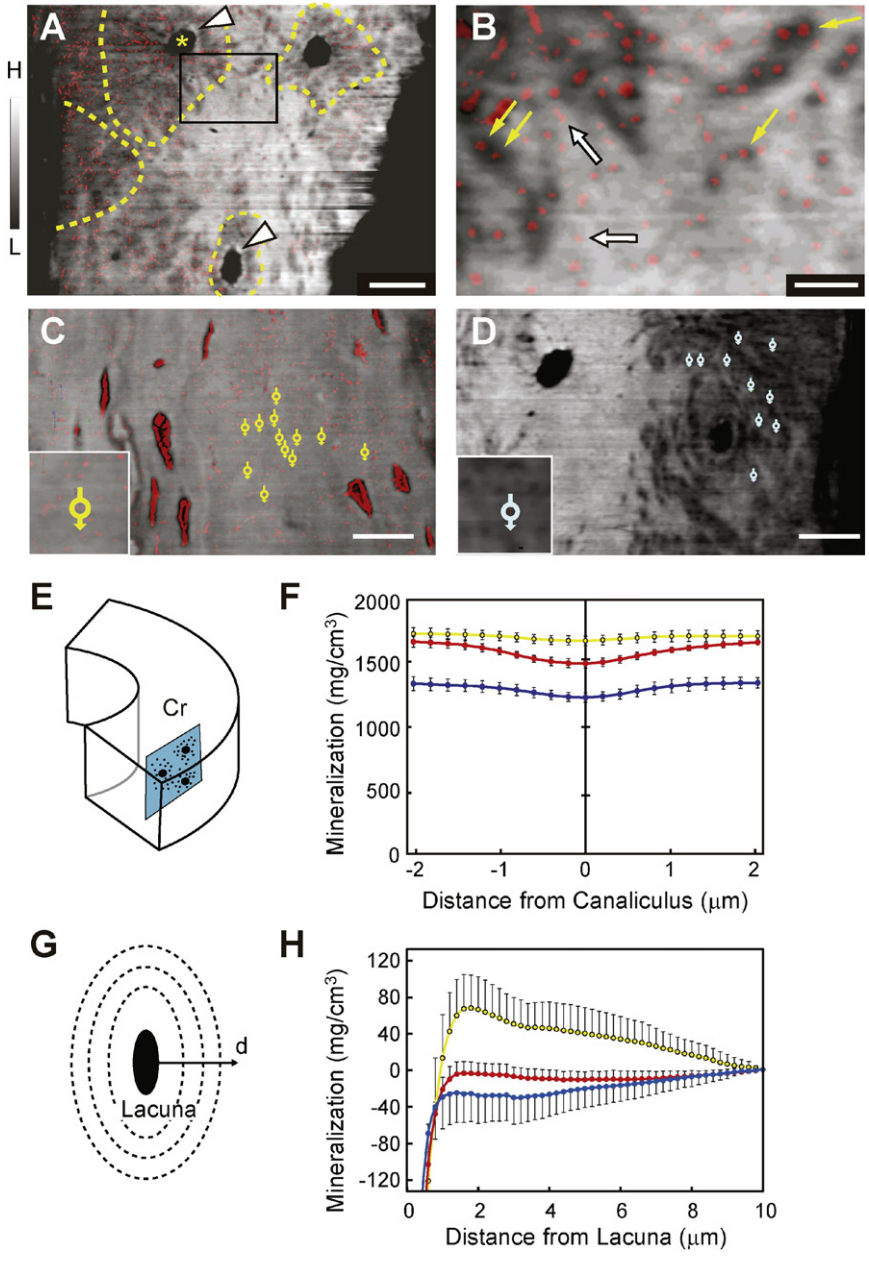

Fig. 3. Coronal section perpendicular to canaliculi. A. An overlaid image of a coronal section of cortical bone 50 μm under the periosteum. The degree of mineralization was visualized by Talbot phase-contrast (grayscale: H, high mineralization; L, low mineralization) and canaliculi position was visualized by defocus phase-contrast (red). Yellow dotted lines: low mineralization zones around osteocyte lacunae. Asterisk, osteocyte lacuna. White arrowheads, peri-lacunar hypermineralization. Scale bar, 20 μm. Boxed area is shown at higher magnification in (B). B. Canaliculus surrounded by low (yellow arrows) and high (white arrows) mineralization. Scale bar, 4 μm. C, D. Canaliculi in high (C) and low (D) mineralization zones. Circles with arrows show positions of canaliculi and the direction of measurement of "distance from canaliculus" and "mineralizaton" in (F). Scale bar, 20 μm. E. Images were generated in a coronal plane (Cr). F. Degree of mineralization across canaliculi in high (yellow, n = 12), intermediate (red, n = 12) and low (blue, n = 12) mineralization zones. Values are presented as means ± SD. G. Schematic presentation of an osteocyte lacuna and the distance (d) from the lacuna surface used in (H). H. Degree of mineralization plotted relative to 10 μm from the lacuna in high (yellow, n = 9), intermediate (red, n = 10) and low (blue, n = 10) mineralization zones. Values are presented as means ± SD.

3.2. Mineral density decreased from the periphery to the canaliculus

We next evaluated the degree of mineralization around canaliculi in a sagittal section, which vertically spanned the endosteal and periosteal surfaces of tibial cortical bone such that a section contained canaliculi longitudinally in the appositional growth region (Fig. 2D). Talbot phase-contrast imaging revealed multiple low mineral areas, including osteocytic lacunae and canaliculi (Fig. 2A), as confirmed by defocus phase-contrast imaging (Fig. 2B). We then quantified the degree of mineralization along a line intersecting the canaliculus at a right angle (indicated as a-b in Fig. 2A). a and b points were 4 μm apart flanking the canaliculus. Quantitative analysis indicated that mineral density decreased from the periphery to the canaliculus in a pattern reminiscent of a V-shaped valley (Fig. 2C). Because canaliculi diameters range from 0.13 to 0.39 μm [12], the diameter (up to 4 μm) of the area with decreased mineral density was 10–30 times greater than the diameter of canaliculi, suggesting that bone mineral is dissolved around a canaliculus, presumably by acid diffusion from dendrites.

3.3. Mneral dissolution starts from the canaliculus

We next analyzed the degree of mineralization in a coronal section parallel to and 50 μm under the periosteal surface. Osteocyte canaliculi crossed perpendicular to the coronal section in the appositional growth region (Fig. 3A-E). We then overlaid an image of canaliculi (red) obtained using the defocus phase-contrast method onto grayscale mineralization levels obtained using Talbot phase-contrast imaging (Fig. 3A, B, C). We observed low mineralization zones around osteocytic lacunae, as indicated by yellow dotted lines in Fig. 3A. Larger low mineralization zones frequently showed lower average mineralization levels than did smaller ones. We also observed lacunae fully or partially surrounded by high peri-lacunar mineralization at the edge (Fig. 3A, arrowheads), suggesting that osteocyte lacunae *per se* are not the center of demineralization. Furthermore, higher magnification views of boxed regions in Fig. 3A showed that most areas of low mineral density were closely associated with the central canaliculi, visualized as red points (Fig. 3B, yellow arrows). By contrast, we also observed canaliculi not associated with decreased mineralization (Fig. 3B, white arrows). Importantly, we observed highly mineralized bone matrix between canaliculi, indicative of peri-canalicular demineralization rather than peri-lacunar demineralization. Transmission electron microscopy analysis of cortical bone also revealed both intact and demineralized bone matrix around a canaliculus (Supplemental Fig. S2).

We quantified the degree of mineralization across canaliculi in high-, intermediate- and low mineralization zones. Examples of canaliculi selected for calculation in high and low mineralization zones

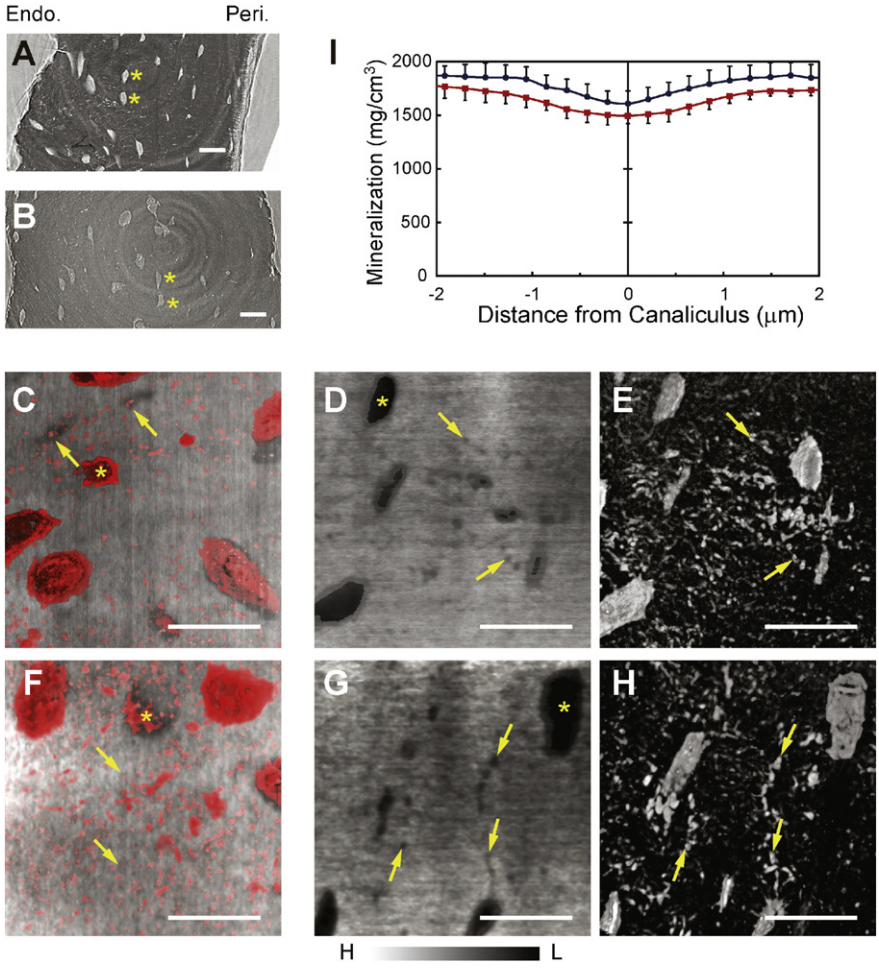

Fig. 4. Mineral dissolution after continuous PTH infusion. A, B. Horizontal sections of tibial cortical bones isolated from control (A) and PTH-infused (B) mice observed by defocus phase-contrast. Endo., endosteum. Peri., periosteum. Asterisks, osteocyte lacuna. C. Coronal section from control. A Talbot phase-contrast image showing mineral density (grayscale: H, high mineralization; L, low mineralization) overlaid with a corresponding defocus phase contrast image showing the lacuno–canalicular system (red). D, E. Sagittal sections for controls. A Talbot phase-contrast image (D) and a defocus phase-contrast image (E). F, G, H. Coronal (F) and sagittal (G, H) sections from PTH-infused animals corresponding to control coronal (C) and sagittal (D, E) sections. Asterisks, osteocyte lacuna. Arrows, canaliculus surrounded by low mineralization in the vicinity of canaliculus. I. Mineralization across the center canaliculus, as quantified in coronal sections. Blue, control mice. Red, PTH-infused mice. Nine canaliculi each were assessed. Values are means ± SD. Scale bars, 20 μm.

are shown in Fig. 3C and D, respectively. On average, in the vicinity of a canaliculus, the degree of mineralization decreased towards its center, particularly in intermediate mineralization zones (Fig. 3F). These data suggest that mineral dissolution starts from the canaliculus, not from the lacuna, and expands concentrically into the surrounding area. We also measured the degree of mineralization around lacunae at various distances from the lacuna (Fig. 3G). Consistent with a previous report [26], osteocytes in high mineralization zones showed peri-lacunar hypermineralization (Fig. 3H, yellow line). By contrast, we found that osteocytes in low mineralization zones with extensive peri-canalicular demineralization are not associated with hypermineralized edges (Fig. 3H, blue line). These data suggest that distant peri-canalicular demineralization precedes demineralization occurring around the lacuna.

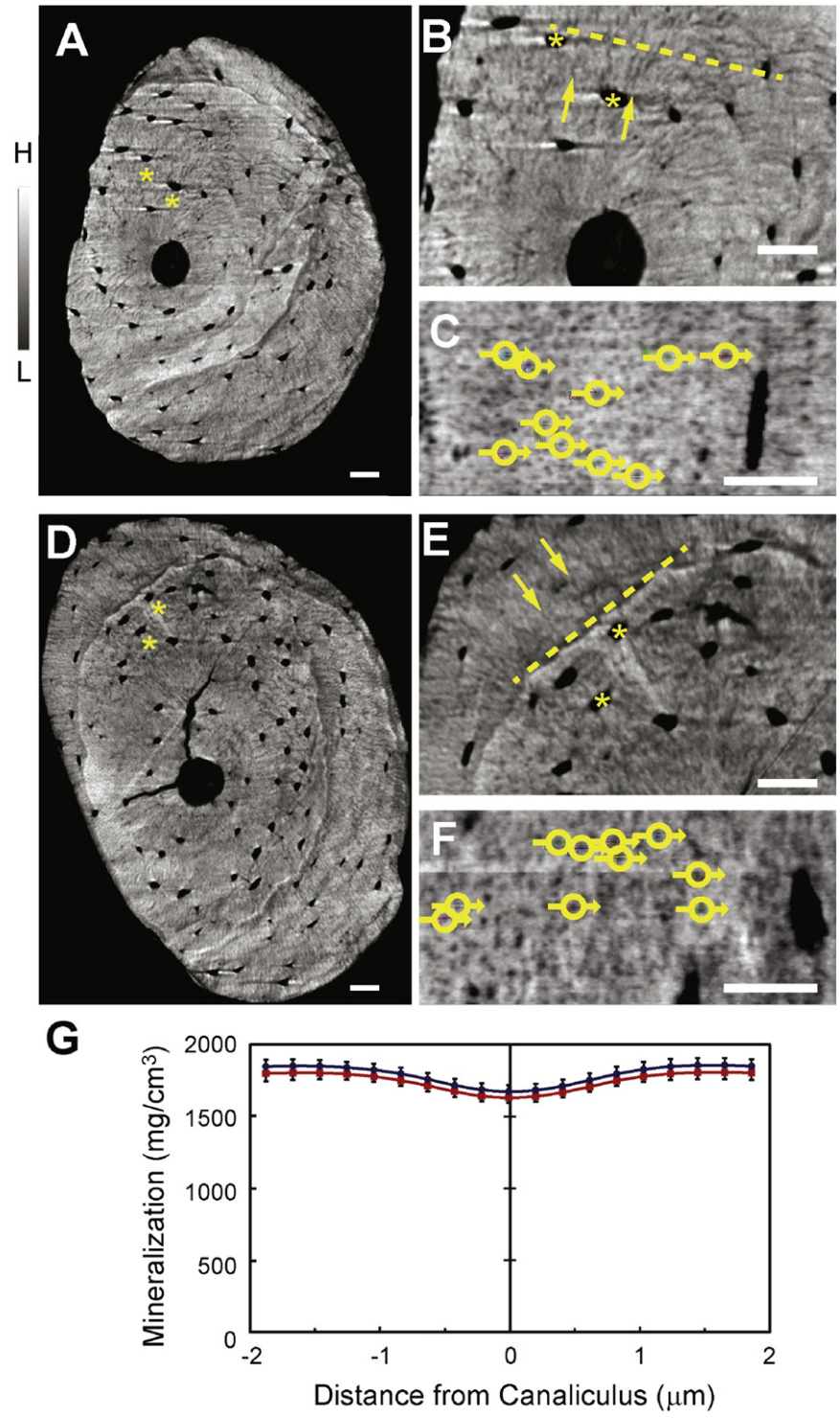

Fig. 5. Mineral dissolution in lactating mice. A, B, C. Talbot phase contrast image (grayscale: H, high mineralization; L, low mineralization) of fibula isolated from control virgin mice. Cross section of fibula at 1 mm proximal to the distal tibiofibular junction (A), and a higher magnification image (B). Dotted line in (B) indicates position of the coronal section (C). Circles with arrows show positions of canaliculi and the direction of mineralization measurement in (G). D, E, F. Lactating mice, corresponding to control panels (A), (B) and (C). Asterisks, osteocyte lacuna. Arrows, osteocyte canaliculus. Six mice in each group showed comparable results. G. Mineralization across the center canaliculus, as measured in coronal sections. Blue, control virgin mice. Red, lactating mice. Ten canaliculi were assessed. Values are means ± SD. Scale bars, 20 μm.

3.4. Peri-canalicular demineralization in PTH-infused mice

To validate peri-canalicular demineralization, we analyzed tibiae of PTH-infused and control animals, since continuous infusion of PTH-related peptide (PTHrP) induces osteocytic remodeling particularly in trabecular bone [17]. Based on analysis of horizontal sections of tibial cortical bone isolated from control (Fig. 4A) and PTH-infused (Fig. 4B) animals, we generated coronal sections of control (Fig. 4C, D and E) and PTH-infused animals (Fig. 4F, G and H) *in silico*. Low mineral density areas were observed in overlay coronal sections (Fig. 4C and F) and in sagittal sections using Talbot-phase contrast (Fig. 4D and G) in the vicinity of the lacuno–canalicular system, as visualized by defocus phase contrast imaging (Fig. 4E and H). PTH-infused mice showed more prominent peri-canalicular mineral dissolution than did controls (Fig. 4I).

3.5. Peri-canalicular demineralization in lactating mice

Loss of peri-lacunar bone matrix reportedly occurs in lactating mice to meet increased calcium demands [17]. Thus we assessed the degree of mineralization around the lacuno–canalicular network in fibulae obtained from virgin (Fig. 5A, B and C) and lactating (Fig. 5D, E and F) mice. Numerous canaliculi running between endosteum and periosteum mediated by osteocyte lacunae were clearly visualized (Fig. 5B and E). Both virgin and lactating mice showed mineral dissolution around osteocyte canaliculi (Fig. 5G).

3.6. Peri-canalicular demineralization in osteopetrotic mice

To determine whether osteoclasts are required for peri-canalicular dissolution, we examined mineral density distribution around canaliculi in osteopetrotic mice, which are devoid of osteoclasts [33]. To do so, we used mutant mice lacking either the transcription factor c-Fos (*Fos*$^{-/-}$ mice) or RANKL (*Tnfsf11*$^{-/-}$ mice), both of which exhibit osteopetrotic phenotypes. Cortical bone from *Fos*$^{-/-}$ mice and respective wild-type controls showed two types of bone matrix, one apparently generated by endochondral ossification and the other by appositional growth. Furthermore, in samples from *Fos*$^{-/-}$ mice (Fig. 6A), we observed low mineral density areas along canaliculi in both coronal (Fig. 6B) and sagittal sections (Fig. 6CD). Canaliculus-centered demineralization was confirmed by quantitative analysis (Fig. 6E). *Tnfsf11*$^{-/-}$ mice also showed peri-canalicular demineralization, albeit at lower frequencies than in *Fos*$^{-/-}$ mice (Supplemental Fig. S3). These analyses support the idea that osteoclasts are dispensable for peri-canalicular demineralization, and that such demineralization is directed by osteocytes.

Finally, we analyzed the connection between the lacuno–canalicular network and intracortical bone canals [34] in the endosteal half of cortical bone. As shown in Fig. 7, multiple osteocyte lacunae (asterisks)

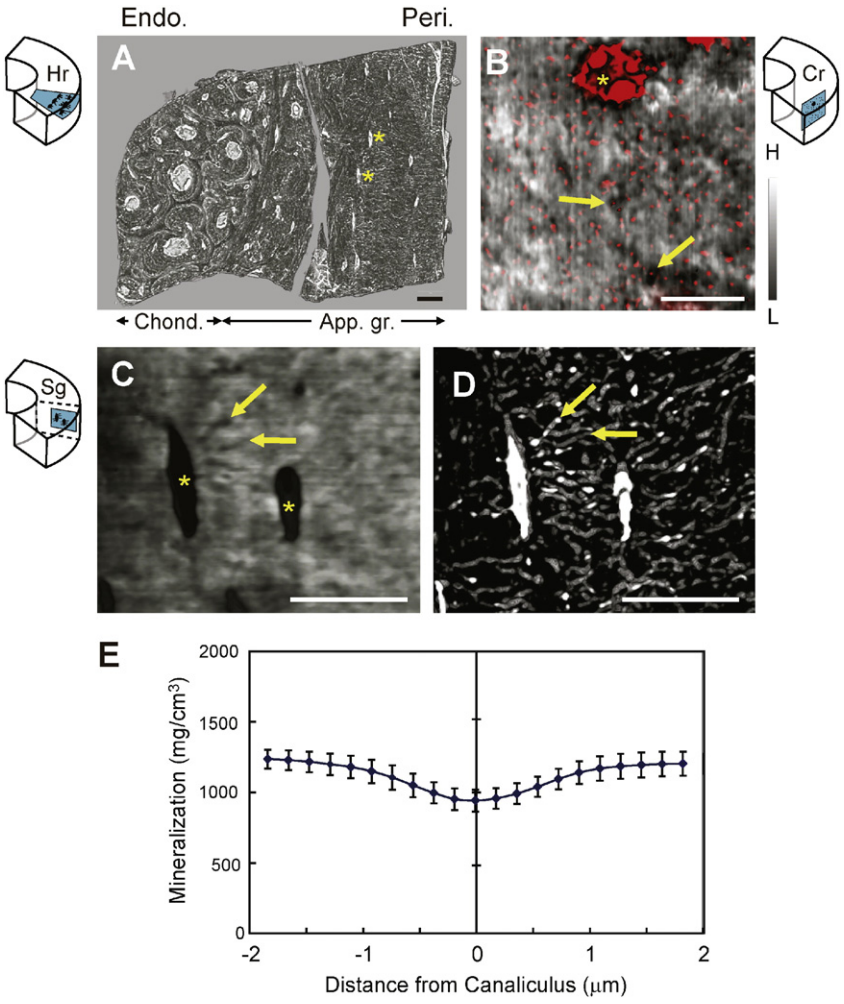

Fig. 6. Mineral dissolution in *Fos*$^{-/-}$ mice. A. Horizontal image of tibial cortex prepared form a 28-week-old *Fos*$^{-/-}$ mouse observed by defocus phase-contrast. Chond., endochondral ossification. App. gr., appositional growth. Endo., endosteum. Peri., periosteum. B. Coronal image of overlaid "degree of mineralization" (grayscale: H, high mineralization; L, low mineralization) and lacuno–canalicular network (red) under the periosteum. C, D. Sagittal section showing degree of mineralization (C) and lacuno–canalicular network (D) in the appositional growth region. Asterisks, osteocyte lacuna. Arrows, osteocyte canaliculus. E. Mineralization across the center canaliculus as measured in coronal sections. Ten canaliculi were measured. Values are means ± SD. Scale bar, 20 μm.

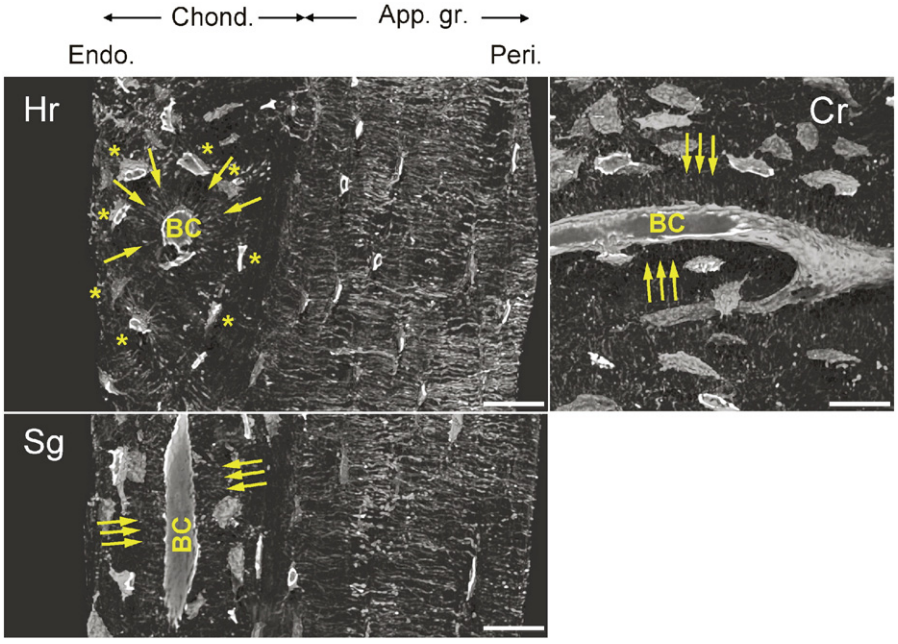

Fig. 7. The lacuno–canalicular-bone canal network. Osteocyte canaliculi are associated with the bone canal (BC) in the endosteal cortex (Chond., endochondral ossification). App. gr., appositional growth. Note that the BC is surrounded by osteocyte lacunae (asterisks), and canaliculi (arrows) run radially from the BC in the center to osteocyte lacunae. Hr, horizontal, Sg, sagittal, Cr, coronal. Endo., endosteum. Peri., periosteum. Scale bar, 20 μm.

surrounded the central bone canal (BC) and canaliculi (arrows) ran between osteocytes and the BC. In the periosteal half of cortical bone, osteocytes extended canaliculi to osteocytes in both neighboring and non-adjacent layers. At both peri- and endosteum, the osteocyte lacuno–canalicular network was connected to bone surfaces (Fig. 7).

4. Discussion

Here, we provide radiological evidence supporting dissolution of bone mineral along osteocyte canaliculi. Synchrotron X-ray tomographic imaging revealed that the degree of peri-canalicular demineralization varied among osteocytes: peri-canalicular demineralization occurred, to various extents, in a manner coordinated by osteocytes from which canaliculi are derived.

Within a single cortical bone sample, we detected zones of high, intermediate, and low mineralization. We observed mineral precipitation at the edge of a lacuna in highly mineralized zones (Fig. 8). Such peri-lacunar hypermineralization persists during peri-canalicular dissolution in the intermediate zones, suggesting that dissolution occurs independently of peri-lacunar resorption. In addition, in the intermediate zone, more highly mineralized background bone matrix was clearly apparent between cylindrical lower mineralization areas around canaliculi, supporting the idea that peri-canalicular dissolution occurs. Peri-canalicular demethylation was more evident in cases of continuous PTH administration or lactation. Peri-lacunar hypermineralization was partially or entirely lost in large low mineralization zones with extensive peri-canalicular dissolution (Fig. 8). Conversely, low mineralization zones may remineralize through active and passive processes [26].

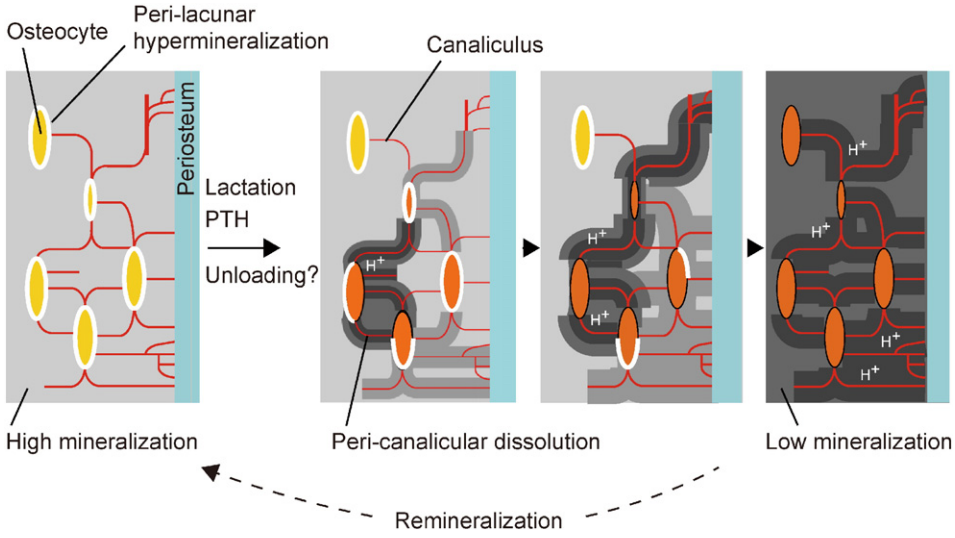

Fig. 8. A model for peri-canalicular demineralization (sagittal section). Peri-canalicular dissolution starts with a subset of osteocytes in high mineral zones. Peri-lacunar hypermineralization is partially or totally lost after peri-canalicular demineralization progresses, giving rise to larger zones of intermediate to low mineralization. Yellow ovals: osteocytes that do not direct demineralization. Red ovals: osteocytes directing peri-canalicular demineralization. High mineralization zones are likely restored by remineralization.

Our data clearly indicate that osteoclasts are not essential for peri-canalicular demineralization. Osteoclasts are localized not only to bone surfaces but within bone matrix, usually near blood vessels contained in bone canals. Furthermore, osteocytes communicate with osteoclasts by producing the osteoclastogenic cytokine RANKL [14]. Therefore, osteoclasts are a potential source of acids that travel through the lacuno–canalicular system. However, since cylindrical peri-canalicular low mineral density regions were also observed in osteopetrotic mice, which lack osteoclasts [33], osteoclasts are dispensable for acidification of osteocyte canaliculi.

Numerous canaliculi run through bone matrix, which consists of hydroxyapatite and organic components such as type I collagen. The total number of canaliculi originating from each lacuna ranges from 41 to 115 in six representative species (chicks, rabbits, humans, and bovine, equine and canine species) [22,35]. In general, the higher the body mass, the lower the density of osteocyte lacunae [36]. For example, osteocyte lacunar density is 17,000/mm^3 for hippopotamus, 20,000/mm^3 for humans [37], and 50,000–66,000/mm^3 in the femoral diaphysis of two mouse strains analyzed [38]. Therefore, assuming a canaliculus diameter of 260 nm and that each lacuna extends 50 canaliculi within a 1-mm cube, the total surface area of canaliculi would be at least 60 mm^2 ($60{,}000^{(2/3)} \times 260 \times 10^{(-6)} \times \pi \times 50$), which is 10-fold greater than the surface of the cube (which would be 6 mm^2). In other words, bone could be resorbed more efficiently from the inside (from the canalicular surface) than from the outside (from the classical bone surface). Since we observed cylindrical low mineral density regions along canaliculi, it is likely that dendrites acidify the surrounding area, solubilize hydroxyapatite, allowing calcium and phosphate ions to enter the lacuno–canalicular system. We observed that canaliculi ran between osteocytes and the central canal, an arrangement that would allow fluid flow between canaliculi and the peripheral bloodstream. This organization is reminiscent of the Harversian system seen in larger mammals [21] or of osteogenic capillaries in mice [39]. Calcium and phosphate ions mobilized by peri-canalicular demineralization likely have access to systemic circulation.

One limitation of this study is that synchrotron X-ray tomographic microscopy does not allow *in vivo* time-course analyses, a capability that may be possible in the future [40]. We thus do not provide direct evidence for the rate of peri-canalicular demineralization or whether it is reversible but rather infer the temporal sequence of events based on snapshots of zones of differing degrees of mineralization (Fig. 8). Quantitative time-course analysis of peri-canalicular demineralization in bones of animals assessed in states of PTH-infusion, lactation, or unloading should reveal whether and how peri-canalicular demineralization is altered by these stimuli.

In summary, here we provide 3D radiological evidence that osteocytes dissolve mineral through canaliculi. Osteocyte dendrites likely possess a mechanism to acidify their microenvironment, dissolve mineral and then transfer it to the bloodstream. Excessive peri-canalicular demineralization could lead to low bone mass and poor bone quality as seen in bone-loss diseases, including osteoporosis.

Supplementary data to this article can be found online at http://dx.doi.org/10.1016/j.bone.2015.12.006.

Acknowledgments

We thank Akihisa Takeuchi, Yoshio Suzuki and Naoto Yagi at the Japan Synchrotron Radiation Research Institute (JASRI/SPring-8) for help with synchrotron X-ray microscopy, and Elise Lamar for critical reading of the manuscript. This work was supported by JSPS KAKENHI Grant Numbers 25293327 and 26670674 to KM, and 19350027 to AM, and in part by the Network Joint Research Center for Materials and Devices. Experiments were performed with approval of the SPring-8 committee (Proposal No. 2009A1195, 2009A1871, 2010B1438, 2012B1316, 2013B1213, 2013B1425).

Authors' roles: Study design: NN, AM and KM. Preparation of samples: NN and SK. Construction of the synchrotron X-ray microscope: WY and AM. Data collection and analysis: NN, SK, WY, AM and KM. Electron microscopy: TH. Manuscript writing: NN, AM and KM.

References

[1] D.E. Clapham, Calcium signaling, Cell 131 (2007) 1047–1058.
[2] L.D. Quarles, Endocrine functions of bone in mineral metabolism regulation, J. Clin. Invest. 118 (2008) 3820–3828.
[3] T.L. Clemens, G. Karsenty, The osteoblast: an insulin target cell controlling glucose homeostasis, J. Bone Miner. Res. 26 (2011) 677–680.
[4] A.M. Parfitt, Osteonal and hemi-osteonal remodeling: the spatial and temporal framework for signal traffic in adult human bone, J. Cell. Biochem. 55 (1994) 273–286.
[5] K. Matsuo, Cross-talk among bone cells, Curr. Opin. Nephrol. Hypertens. 18 (2009) 292–297.
[6] L.G. Raisz, Pathogenesis of osteoporosis: concepts, conflicts, and prospects, J. Clin. Invest. 115 (2005) 3318–3325.
[7] P. Sambrook, C. Cooper, Osteoporosis, Lancet 367 (2006) 2010–2018.
[8] K. Inoue, T. Hamano, N. Nango, I. Matsui, K. Tomida, S. Mikami, N. Fujii, C. Nakano, Y. Obi, A. Shimomura, Y. Kusunoki, H. Rakugi, Y. Isaka, Y. Tsubakihara, Multidetector-row computed tomography is useful to evaluate the therapeutic effects of bisphosphonates in glucocorticoid-induced osteoporosis, J. Bone Miner. Metab. 32 (2014) 271–280.
[9] L.F. Bonewald, The amazing osteocyte, J. Bone Miner. Res. 26 (2011) 229–238.
[10] S.L. Dallas, L.F. Bonewald, Dynamics of the transition from osteoblast to osteocyte, Ann. N. Y. Acad. Sci. 1192 (2010) 437–443.
[11] T.A. Franz-Odendaal, B.K. Hall, P.E. Witten, Buried alive: how osteoblasts become osteocytes, Dev. Dyn. 235 (2006) 176–190.
[12] L.D. You, S. Weinbaum, S.C. Cowin, M.B. Schaffler, Ultrastructure of the osteocyte process and its pericellular matrix, Anat. Rec. A: Discov. Mol. Cell. Evol. Biol. 278 (2004) 505–513.
[13] J.Q. Feng, L.M. Ward, S. Liu, Y. Lu, Y. Xie, B. Yuan, X. Yu, F. Rauch, S.I. Davis, S. Zhang, H. Rios, M.K. Drezner, L.D. Quarles, L.F. Bonewald, K.E. White, Loss of DMP1 causes rickets and osteomalacia and identifies a role for osteocytes in mineral metabolism, Nat. Genet. 38 (2006) 1310–1315.
[14] K. Matsuo, Osteocytes communicate with osteoclast lineage cells via RANKL, IBMS BoneKEy 9 (2012) 39.
[15] D. Padhi, G. Jang, B. Stouch, L. Fang, E. Posvar, Single-dose, placebo-controlled, randomized study of AMG 785, a sclerostin monoclonal antibody, J. Bone Miner. Res. 26 (2011) 19–26.
[16] N.E. Lane, W. Yao, M. Balooch, R.K. Nalla, G. Balooch, S. Habelitz, J.H. Kinney, L.F. Bonewald, Glucocorticoid-treated mice have localized changes in trabecular bone material properties and osteocyte lacunar size that are not observed in placebo-treated or estrogen-deficient mice, J. Bone Miner. Res. 21 (2006) 466–476.
[17] H. Qing, L. Ardeshirpour, P.D. Pajevic, V. Dusevich, K. Jahn, S. Kato, J. Wysolmerski, L.F. Bonewald, Demonstration of osteocytic perilacunar/canalicular remodeling in mice during lactation, J. Bone Miner. Res. 27 (2012) 1018–1029.
[18] H. Sano, J. Kikuta, M. Furuya, N. Kondo, N. Endo, M. Ishii, Intravital bone imaging by two-photon excitation microscopy to identify osteocytic osteolysis in vivo, Bone 74 (2015) 134–139.
[19] R. Müller, Hierarchical microimaging of bone structure and function, Nat. Rev. Rheumatol. 5 (2009) 373–381.
[20] D.J. Webster, P. Schneider, S.L. Dallas, R. Müller, Studying osteocytes within their environment, Bone 54 (2013) 285–295.
[21] A. Pacureanu, M. Langer, E. Boller, P. Tafforeau, F. Peyrin, Nanoscale imaging of the bone cell network with synchrotron X-ray tomography: optimization of acquisition setup, Med. Phys. 39 (2012) 2229–2238.
[22] P. Dong, A. Pacureanu, M.A. Zuluaga, C. Olivier, F. Frouin, Q. Grimal, F. Peyrin, A new quantitative approach for estimating bone cell connections from nano-CT images, Conf. Proc. IEEE Eng. Med. Biol. Soc. 2013 (2013) 3694–3697.
[23] K.S. Mader, P. Schneider, R. Müller, M. Stampanoni, A quantitative framework for the 3D characterization of the osteocyte lacunar system, Bone 57 (2013) 142–154.
[24] M. Kerschnitzki, P. Kollmannsberger, M. Burghammer, G.N. Duda, R. Weinkamer, W. Wagermaier, P. Fratzl, Architecture of the osteocyte network correlates with bone material quality, J. Bone Miner. Res. 28 (2013) 1837–1845.
[25] Y. Carter, C.D. Thomas, J.G. Clement, A.G. Peele, K. Hannah, D.M. Cooper, Variation in osteocyte lacunar morphology and density in the human femur—a synchrotron radiation micro-CT study, Bone 52 (2013) 126–132.
[26] B. Hesse, P. Varga, M. Langer, A. Pacureanu, S. Schrof, N. Mannicke, H. Suhonen, P. Maurer, P. Cloetens, F. Peyrin, K. Raum, Canalicular network morphology is the major determinant of the spatial distribution of mass density in human bone tissue: evidence by means of synchrotron radiation phase-contrast nano-CT, J. Bone Miner. Res. 30 (2014) 346–356.
[27] N. Nango, S. Kubota, A. Takeuchi, Y. Suzuki, W. Yashiro, A. Momose, K. Matsuo, Talbot-defocus multiscan tomography using the synchrotron X-ray microscope to study the lacuno–canalicular network in mouse bone, Biomed. Opt. Express 4 (2013) 917–923.
[28] Z.Q. Wang, C. Ovitt, A.E. Grigoriadis, U. Möhle-Steinlein, U. Rüther, E.F. Wagner, Bone and haematopoietic defects in mice lacking c-*fos*, Nature 360 (1992) 741–745.
[29] Y.Y. Kong, H. Yoshida, I. Sarosi, H.L. Tan, E. Timms, C. Capparelli, S. Morony, A.J. Oliveira-dos-Santos, G. Van, A. Itie, W. Khoo, A. Wakeham, C.R. Dunstan, D.L. Lacey, T.W. Mak, W.J. Boyle, J.M. Penninger, OPGL is a key regulator of osteoclastogenesis, lymphocyte development and lymph-node organogenesis, Nature 397 (1999) 315–323.
[30] A. Momose, T. Takeda, Y. Itai, K. Hirano, Phase-contrast X-ray computed tomography for observing biological soft tissues, Nat. Med. 2 (1996) 473–475.

[31] Y. Takeda, W. Yashiro, T. Hattori, A. Takeuchi, Y. Suzuki, A. Momose, Differential phase X-ray imaging microscopy with X-ray Talbot interferometer, Appl. Phys. Express 1 (2008) 117002.
[32] A.G. Robling, K.M. Duijvelaar, J.V. Geevers, N. Ohashi, C.H. Turner, Modulation of appositional and longitudinal bone growth in the rat ulna by applied static and dynamic force, Bone 29 (2001) 105–113.
[33] E.F. Wagner, K. Matsuo, Signalling in osteoclasts and the role of Fos/AP1 proteins, Ann. Rheum. Dis. 62 (Suppl. 2) (2003) (ii83-5).
[34] P. Schneider, R. Voide, M. Stampanoni, L.R. Donahue, R. Müller, The importance of the intracortical canal network for murine bone mechanics, Bone 53 (2013) 120–128.
[35] T. Beno, Y.J. Yoon, S.C. Cowin, S.P. Fritton, Estimation of bone permeability using accurate microstructural measurements, J. Biomech. 39 (2006) 2378–2387.
[36] K.W. Stein, J. Werner, Preliminary analysis of osteocyte lacunar density in long bones of tetrapods: all measures are bigger in sauropod dinosaurs, PLoS One 8 (2013), e77109.
[37] T.G. Bromage, R.S. Lacruz, R. Hogg, H.M. Goldman, S.C. McFarlin, J. Warshaw, W. Dirks, A. Perez-Ochoa, I. Smolyar, D.H. Enlow, A. Boyde, Lamellar bone is an incremental tissue reconciling enamel rhythms, body size, and organismal life history, Calcif. Tissue Int. 84 (2009) 388–404.
[38] P. Schneider, M. Stauber, R. Voide, M. Stampanoni, L.R. Donahue, R. Müller, Ultrastructural properties in cortical bone vary greatly in two inbred strains of mice as assessed by synchrotron light based micro- and nano-computed tomography, J. Bone Miner. Res. 22 (2007) 1557–1570.
[39] K. Matsuo, Y. Kuroda, N. Nango, K. Shimoda, Y. Kubota, M. Ema, L. Bakiri, E.F. Wagner, Y. Takeda, W. Yashiro, A. Momose, Osteogenic capillaries orchestrate growth plate-independent ossification of the malleus, Development 142 (2015) 3912–3920.
[40] I.V. Pratt, G. Belev, N. Zhu, L.D. Chapman, D.M. Cooper, In vivo imaging of rat cortical bone porosity by synchrotron phase contrast micro computed tomography, Phys. Med. Biol. 60 (2015) 211–232.